Published in final edited form as:
Epilepsia. 2012 June ; 53(0 1): 150–160. doi:10.1111/j.1528-1167.2012.03486.x.

Abnormal dendrite and spine morphology in primary visual cortex in the CGG knock-in mouse model of the fragile X premutation

Robert F. Berman[*,†], **Karl D. Murray**[‡], **Gloria Arque**[*,†], **Michael R. Hunsaker**[*,†], and **H. Jürgen Wenzel**[*,†]

[*]Department of Neurological Surgery, School of Medicine, University of California, Davis, California, U.S.A

[†]Neurotherapeutic Research Institute, School of Medicine, University of California, Davis, California, U.S.A

[‡]Department of Psychiatry and Behavioral Sciences, School of Medicine, University of California, Davis, California, U.S.A

Summary

The fragile X mental retardation 1 gene (*Fmr1*) is polymorphic for CGG trinucleotide repeat number in the 5′-untranslated region, with repeat lengths <45 associated with typical development and repeat lengths >200 resulting in hypermethylation and transcriptional silencing of the gene and mental retardation in the fragile X Syndrome (FXS). Individuals with CGG repeat expansions between 55 and 200 are carriers of the fragile X premutation (PM). PM carriers show a phenotype that can include anxiety, depression, social phobia, and memory deficits. They are also at risk for developing fragile X–associated tremor/ataxia syndrome (FXTAS), a late onset neurodegenerative disorder characterized by tremor, ataxia, cognitive impairment, and neuropathologic features including intranuclear inclusions in neurons and astrocytes, loss of Purkinje cells, and white matter disease. However, very little is known about dendritic morphology in PM or in FXTAS. Therefore, we carried out a Golgi study of dendritic complexity and dendritic spine morphology in layer II/III pyramidal neurons in primary visual cortex in a knock-in (KI) mouse model of the PM. These CGG KI mice carry an expanded CGG trinucleotide repeat on *Fmr1*, and model many features of the PM and FXTAS. Compared to wild-type (WT) mice, CGG KI mice showed fewer dendritic branches proximal to the soma, reduced total dendritic length, and a higher frequency of longer dendritic spines. The distribution of morphologic spine types (e.g., stubby, mushroom, filopodial) did not differ between WT and KI mice. These findings demonstrate that synaptic circuitry is abnormal in visual cortex of mice used to model the PM, and suggest that such changes

Address correspondence to Robert F. Berman, Ph.D., Department of Neurological Surgery, School of Medicine, University of California, One Shields Ave., Davis, CA 95616, U.S.A. rfberman@ucdavis.edu.

Disclosure

The authors have no conflicts of interest.

We confirm that we have read the Journal's position on issues involved in ethical publication and affirm that this report is consistent with those guidelines.

may underlie neurologic features found in individuals carrying the PM as well as in individuals with FXTAS.

Keywords

Golgi impregnation; Pyramidal neurons; Visual cortex; Dendritic spines; Fragile X; Fragile X mental retardation protein; Fragile X premutation; FXTAS; Synapse; Circuitry

---

The fragile X mental retardation gene (*Fmr1*) is located on the long arm of the X chromosome at position q27.3. The gene codes for the fragile X mental retardation protein (FMRP), which is critical for normal synapse formation and synaptic plasticity (Braun & Segal, 2000; Huber et al., 2002; Antar et al., 2006; Bassell & Warren, 2008). The gene contains a CGG trinucleotide repeat expansion of variable length in the 5′-untranslated region (5′-UTR), with normal individuals having repeat lengths between 5 and 45 CGG repeats and normal levels of FMRP. Individuals with CGG repeat expansions >200, referred to as full mutation (FM) carriers, have an absence of FMRP due to hypermethylation and transcriptional silencing of *Fmr1*. These individuals develop fragile X syndrome (FXS) associated with abnormal development of the nervous system and mental retardation. In between normal individuals and carriers of the full mutation are premutation (PM) carriers, who have CGG repeat expansions between 55 and 200. PM carriers are relatively common in the general population, with approximately 1 in 178–250 females and 1 in 400–800 males (Jacquemont et al., 2004; Hagerman, 2008; Hantash et al., 2011).

Premutation carriers were originally thought be unaffected by the premutation. However, it is now established that they show a wide range of neurologic and psychological problems, including anxiety, depression, and subtle motor and cognitive impairments (Berry-Kravis et al., 2007b; Bourgeois et al., 2009; Keri & Benedek, 2010; Kogan & Cornish, 2010; Lachiewicz et al., 2010; Basuta et al., 2011; Goodrich-Hunsaker et al., 2011a,b,c). They also show an increased incidence of seizure disorders (Chonchaiya et al., 2012). In addition, approximately 30% of male PM and 8–11% of female PM carriers older than the age of 50 will develop the neurodegenerative disorder fragile X-associated tremor/ ataxia syndrome (FXTAS), meaning that as many as 1 in 3,000 male individuals in the general population may develop clinical features of FXTAS at some point in their lives (Jacquemont et al., 2004; Hagerman & Hagerman, 2008). FXTAS represents the most severe clinical presentation associated with the PM. Core features include intention tremor and/or ataxia and gradual cognitive decline beginning with memory and executive function leading to dementia and early death in some patients. The majority of patients develop neuropsychiatric problems including depression, anxiety, and cognitive impairment (Hagerman et al., 2001; Berry-Kravis et al., 2007a; Bourgeois et al., 2007; Leehey et al., 2008). Female PM carriers also present with FXTAS, although the movement disorder is less severe, presumably due to the protective effect of the second normal X chromosome (Hagerman et al., 2004; Jacquemont et al., 2004).

Neuropathology includes the presence of intranuclear protein inclusions in neurons and astrocytes in postmortem brain tissue from FXTAS and PM patients. Systematic analysis of these inclusions shows the presence of >20 proteins including ubiquitin, molecular

chaperone Hsp40, 20S proteasome complex, and DNA repair-ubiquitin-associated HR23B, but never FMRP (Tassone et al., 2004; Iwahashi et al., 2006). Of interest, the inclusions contain *FMR1* RNA, but not FMRP (Iwahashi et al., 2006). There is also Purkinje cell loss in the cerebellum, and evidence of white matter disease in major fiber tracts (white matter hyperintensities in T_2-weighted magnetic resonance imaging [MRI] (Brunberg et al., 2002; Greco et al., 2006; Iwahashi et al., 2006). Molecular findings in PM carriers with and without FXTAS include three- to eight-fold elevations in *Fmr1* mRNA in leukocytes and less than threefold in brain tissue, whereas FMRP levels are only slightly reduced by 10–30% (Hessl et al., 2005). Elevated *Fmr1* mRNA has led to the proposal that FXTAS results from a toxic “RNA gain of function” (Hagerman et al., 2001; Jin et al., 2003; Handa et al., 2005), where neuropathology thought to result from the sequestration of RNA-binding proteins important for normal cellular functions (e.g., protein trafficking, alternative splicing, microRNA processing) by the elevated *Fmr1* mRNA (Willemsen et al., 2011). However, cellular mechanisms responsible for elevated *Fmr1* mRNA levels and the pathways that lead to toxicity remain largely unknown (Raske & Hagerman, 2009).

To investigate the pathologic and behavioral consequences of the fragile X premutation, a transgenic CGG knock-in (KI) mouse was developed in which a native eight CGG repeat in the endogenous murine *Fmr1* gene was replaced via homologous recombination with an expanded 98 CGG repeat of human origin. The CGG repeat expansion shows modest instability across generations, so that separate lines of CGG KI mice have been generated with repeat expansions ranging from 70 to >300 (Willemsen et al., 2003; Berman & Willemsen, 2009). As summarized in Table 1, these mice model much of the pathophysiology and behavioral deficits found in the PM and FXTAS patients, including two- to threefold elevated *Fmr1* mRNA levels in brain and 10–30% reduction in FMRP expression (Bontekoe et al., 2001; Tassone et al., 2007; Brouwer et al., 2008). In addition, both human FXTAS patients and the CGG KI mouse show ubiquitin-positive intranuclear inclusions in neurons and astrocytes (Fig. 1), a key neuropathologic feature of FXTAS in humans (Greco et al., 2006; Wenzel et al., 2010).

Although a great deal is known about the gross neuropathology associated with PM carriers, little is known about abnormal dendritic and synaptic morphology that may underlie some of the cognitive deficits associated with the PM and FXTAS. Therefore, the present study used a modified Golgi-Cox impregnation to examine dendritic branching complexity and spine density and morphology associated with the PM and FXTAS in the visual cortex of a CGG KI mouse model of the PM (Willemsen et al., 2003; Van Dam et al., 2005). Compared to WT mice, CGG KI mice showed fewer dendritic branches proximal to the soma, reduced total dendritic length, and longer dendritic spines. The distribution of morphologic spine types (e.g., stubby, mushroom, filopodial) did not differ between WT and KI mice. These findings demonstrate that synaptic circuitry is abnormal in visual cortex of mice used to model the fragile X premutation, and suggest that such changes may underlie some of the neurologic features found in individuals carrying the premutation as well as in individuals with FXTAS.

Methods

Subjects

The CGG KI mice used in this study were bred at UC Davis and were congenic on a C57BL/6J background. They were generated by backcrossing mice initially on a mixed FVB/N × C57BL/6J onto a C57BL/6J background over >12 generations (Willemsen et al., 2003; Wenzel et al., 2010). Mice were housed in same-sex groups with three or four mice per cage in a temperature- and humidity- controlled vivarium on a 12 h light-dark cycle. Mice had ad libitum access to food and water. All experiments were conducted under a research protocol approved by the Institutional Care and Use Committee at the University of California Davis.

Genotyping

Genotyping of CGG KI and WT mice was carried out on DNA extracted from tail snips. Briefly, tails were incubated overnight at 55°C with 10 mg/ml Proteinase K (Roche Diagnostics, Mannheim, Germany) in 300 μl lysis buffer containing 50 mM Tris–HCl, pH 7.5, 10 mM ethylenediaminetetraacetic acid, 150 mM NaCl, 1% sodium dodecyl sulfate. One hundred microliters saturated NaCl was then added and the suspension was centrifuged. One volume of 100% ethanol was added and gently mixed, and the DNA was pelleted by centrifugation and the supernatant discarded. The DNA was washed and centrifuged in 500 μl 70% ethanol. The DNA was then dissolved in 100-μl MilliQ-H_2O. CGG repeat lengths were determined by polymerase chain reaction (PCR) using the Expanded High Fidelity Plus PCR System (Roche Diagnostics, Indianapolis, IN, U.S.A.). Briefly, approximately 500– 700 ng of DNA was added to 50 μl of PCR mixture containing 2.0 μM of each primer, 250 μM of each dNTP (Invitrogen, Tigard, OR, U.S.A.), 2% dimethyl sulfoxide (Sigma-Aldrich, St. Louis, MO, U.S.A.), 2.5 M Betaine (Sigma-Aldrich), 5 U Expand HF buffer with mg (7.5 μM). The forward primer was 5′-GCTCAGCTCCGTTTCGGTTTCACTTCCGGT-3′ and the reverse primer was 5′-AGCCCCGCACTTCCACCACCAGCTCCTCCA-3′. PCR steps were 10 min denaturation at 95°C, followed by 34 cycles of 1 min denaturation at 95°C, annealing for 1 min at 65°C, and elongation for 5 min at 75°C to end each cycle. PCR ends with a final elongation step of 10 min at 75°C. DNA CGG repeat band sizes were determined by running DNA samples on a 2.5% agarose gel and staining DNA with ethidium bromide. Genotyping was performed twice on each animal, once using tail snips taken at weaning and again on tail snips collected at the time of sacrifice. In all cases the genotypes matched.

Golgi analysis and neuronal reconstruction

Neuronal architecture was assessed on tissue processed for Golgi stain by a modified Golgi-Cox impregnation method using the FD RapidGolgi stain kit according to manufacturer's instructions (FD NeuroTechnologies, Columbia, MD, U.S.A.). Briefly, 5–10 mm blocks of tissue were isolated following rapid removal of brain from scull and immersed in a mercuric chloride, potassium dichromate, and potassium chromate solution for approximately 2 weeks at room temperature in the dark. Subsequently, tissue blocks were vibratome sectioned at 80–100 μM thickness, mounted onto glass slides, and stained by exposure to

NH_4OH solution. A total of 26 neurons from eight CCG KI mice and 27 neurons from eight WT control mice were used for quantitative analysis.

Dendritic complexity and the neuronal spine density of layer II/III neurons in primary visual cortex of CGG KI and littermate WT mice was measured from whole cell reconstructions using Neurolucida software (MBF Bioscience, Williston, VT, U.S.A.) on a Zeiss Axioscope 100 microscope (Carl Zeiss, Thornwood, NY, U.S.A.) with motorized stage and a color CCD camera. Dendrites were drawn at high magnification through a Zeiss Apochromat 100×, 1.4 NA, oil immersion lens. A total of 50 cells from 16 animals (eight CGG KI and eight WT littermate controls) were processed for measures of dendritic complexity. Neurons were chosen for analysis based on the following criteria: (1) the quality of Golgi impregnation; (2) the relative isolation of impregnated neurons compared with neighboring impregnated cells; and (3) the position of neurons within primary visual cortex (V1) and layer II/III as determined by reference to Nissl-stained tissue sections from littermate animals. Complete reconstructions of apical and basilar dendritic fields were performed using Neurolucida for each neuron, and measures of dendritic length, volume, tortuosity, and branch order were obtained. Branch order was assigned using the centrifugal scheme. In addition, dendritic complexity was assessed by Sholl analysis (Sholl, 1953). Here, a series of concentric rings of consistently increasing size are centered over the cell soma and the number of dendritic crossings is measured at each ring. Dendritic trees with more branches will have increased numbers of ring crossings, thus providing a quantitative assessment of complexity.

To measure spine densities, complete reconstructions from separate cells of single apical and basal dendritic branches with spines marked were obtained from five CGG KI and six littermate WT mice. Dendritic branches were drawn at high magnification (Zeiss Apochromat 100×, 1.4 NA, oil immersion lens) using Neurolucida software along the whole dendrite from the cell soma to the tips of branches, and spines were classified according to their morphology (filipodial, stubby, or mushroom). In total, 1,096 spines from five CGG KI mice and 1,310 spines from five WT littermate control mice were measured and data regarding length, volume, and number of spines were obtained.

Western blot analysis of FMRP

Mice were sacrificed by cervical dislocation, and brains were rapidly removed, frozen, and stored at −80°C. WT (n = 5) and CGG KI (n = 12) mice with CGG repeat lengths ranging between 84–210 (mean 138.6 ± 12.0) were used. Samples were homogenized in N-2-hydroxyethylpiperazine-N′-2-ethane sulfonic acid buffer with protease inhibitor cocktail (Roche Diagnostics). Protein concentrations were determined and 60 μg of the protein extracts were diluted with Laemmli sample buffer (Bio-Rad, Hercules, CA, U.S.A.), heated for 5 min at 98°C and loaded onto an 8% sodium dodecyl sulfate polyacrylamide gel electrophoresis gel. The proteins were transferred onto nitrocellulose membranes. The membranes were blocked with LiCor Odyssey Imaging System (LiCor Biosciences, Lincoln, NE, U.S.A.) blocking buffer for 2 h. They were incubated overnight at room temperature with primary antibodies specific for FMRP (1:20,000, polyclonal chicken host, (Iwahashi et al., 2009). Immunoreactivity against beta actin (1:10,000, monoclonal mouse

host; Sigma-Aldrich, St. Louis, MO, U.S.A.) served as a loading control and was used to normalize protein concentrations between gels and lanes. Membranes were incubated for 1 h at room temperature with secondary antibodies (donkey anti-chicken 800 IR-Dye 1:10,000 and goat antimouse 680 IR-Dye 1:10,000; LiCor Odyssey Imaging System), followed by several washes. The levels of FMRP and Actin were quantified using the LiCor Odyssey Imaging System software.

Fmr1 mRNA levels quantified by quantitative reverse-transcription polymerase chain reaction

RNA isolation from whole brain was performed according to Brouwer et al. (2008). RNA concentration and purity was determined using a NanoDrop ND-1000 Spectrophotometer (NanoDrop Technologies, Thermo Scientific, Wilmington, DE, U.S.A.). RNA (1 ng) was reverse transcripted using an iScript kit (Bio-Rad) according to manufacturer's instructions. Quantitative qPCR (qPCR) was performed on a TaqMan real-time PCR instrument (ABI 7900; Applied Biosystems, Foster City, CA, U.S.A.) using TaqMan PCR chemistry that specifically utilizes the 5′-nuclease activity of the Taq polymerase to cleave a reporter probe to release a fluorescent dye from its quencher molecule. The change in fluorescence can be measured in real-time. Each qPCR was performed in duplicate with three starting RNA concentrations (25, 12.5, and 6.25 ng), for both the target gene (*Fmr1*) and a housekeeping gene glucoronidase (*GUS*) (a total of 12 reactions). Five microliters of complimentary DNA (cDNA) was then used as template in a qPCR reaction with the following TaqMan probes: Forward-FMR1 5′-GCA GAT TCC ATT TCA TGA TGT CA-3 and Reverse-FMR1, 5′-ACC ACC AAC AGC AAG GCT CT-3′. Forward-GUS, 5′-CTC ATT TGG AAT TTT GCC GAT T-3′; reverse-GUS, 5′-CCG AGT GAA GAT CCC CTT TTT A-3′ (ABI PRISM 7900 HTA FAST Sequence Detector System). A pool of mRNA from adult WT mice was used as an internal and interplate control. C_t values of GUS were subtracted from the C_t value of *Fmr1* gene for each sample, which gives the ΔC_t. ΔC_t of WT was then subtracted from ΔC_t of CGG mice, which is designated as the $\Delta\Delta C_t$. $2-\Delta\Delta C_t$ then gives fold change. Samples were standardized in an intraplate manner and interplate manner.

Data analysis

Data are expressed as means ± standard error of the mean (SEM). For quantitative measures of dendritic reconstructions, traces were exported into Neuroexplorer (MBF Bioscience). Statistical significance of grouped dendritic and spine measures between CGG KI and WT mice were determined using a two-tailed Student's *t*-test. For comparisons of differences using the Sholl analysis, the number of intersections at defined distances from the soma was compared between CGG KI and littermate WT mice using a two-tailed Student's *t*-test. Significance in the cumulative distribution plots for spine densities was determined using the nonparametric two sample Kolmogorov-Smirnov test (Stratford et al., 1997). *Fmr1* mRNA expression and FMRP levels were analyzed statistically using a one-way ANOVA. The minimum level of statistical significance for all tests was set at $\alpha = 0.05$.

Results

Individual layer II/III pyramidal neurons in visual cortex were visualized using a Nikon E600 brightfield microscope with a 100× oil immersion objective and motorized stage. Soma and apical and basilar dendrites were then traced for selected neurons using Neurolucida software (MBF Bioscience) as shown in Fig. 2 for a representative WT mouse with a normal 8–10 CGG repeat length and a representative CGG KI mouse with a 156 CGG repeat expansion. Dendritic complexity was quantified by Sholl analysis by counting the number of branch intersections with concentric rings progressively increasing by 20 μm. As shown in Fig. 3, the number of ring intersections was generally lower in CGG KI mice compared to WT mice, and significantly lower at 40 μm ($p < 0.05$). Dendritic length was also calculated from Neurolucida reconstructions (Fig. 4). When calculated across both apical and basilar dendrites, total dendritic length was significantly shorter in CGG KI mice compared to WT mice. However, when examined separately, the decrease in dendritic length was found to be significant for apical but not basilar dendrites.

Spine length was also quantified in layer II/III pyramidal neurons in primary visual cortex for both basilar and apical dendritic spines (Fig. 5). Spine length is expressed as the cumulative frequency of spine lengths binned in 0.4-μm segments. The range of spine lengths observed in pyramidal neurons ranged between 0.4 and 5.0 μm. As shown in Fig. 5, the cumulative frequency of basilar spine lengths for CGG KI mice was shifted significantly to the left ($p < 0.05$), demonstrating an increase in the frequency of longer dendritic spines compared to WT mice. In contrast, there was no difference in distribution of spine lengths for apical spines.

As shown in Fig. 6, spine density was also quantified for all spines visualized as well as for three different spine submorphologies, based on a modification of previous classification schemes described earlier (Irwin et al., 2001). The three morphologic subgroups were stubby and mushroom shape reflecting mature spines, and long and spindly filipodial spines for immature appearing spines. However, there were no significant differences in spine density when summed across all spines or when examined within mature or immature spine groups.

A characteristic molecular finding in the brains of CGG KI mice is a 1.5–3 fold increase in brain *Fmr1* mRNA expression, and a 15–50% reduction in brain levels of FMRP due in part to translational inefficiency of *Fmr1* mRNA bearing an expanded CGG repeat expansion (Brouwer et al., 2008). Therefore, *Fmr1* mRNA expression and FMRP levels in whole brain were quantified in a separate group of CGG KI and WT mice of similar age to those used for Golgi analysis in order to establish that the mice bred for use in this study showed the expected molecular features. As shown in Fig. 7, average *Fmr1* mRNA expression was increased by approximately 1.4 fold in the brains of mice compared to WT mice ($p < 0.05$), whereas levels of FMRP were reduced by 28% in the brains of CGG KI mice versus WT mice.

Discussion

Pyramidal neurons in layers II/III of primary visual cortex of CGG KI mice showed less complex dendritic branching patterns, reduced total dendritic length (apical dendrites), and longer dendritic spines on basal dendrites. These results extend earlier studies showing histopathology in CGG KI mice (e.g., intranuclear inclusions) to include abnormalities in the fine structure of dendrites and dendritic spines. They also suggest that dendritic branching and spine morphology may be abnormal in PM carriers and FXTAS patients, although this has not yet been demonstrated. These findings are important because reduced dendrite complexity and altered spine morphology could underlie, at least in part, behavioral impairments reported in CGG KI mice. These impairments include processing of visual spatial information (Hunsaker et al., 2009), temporal information (Hunsaker et al., 2010), and poor visual-motor coordination in a test of locomotor coordination (Hunsaker et al., 2011).

The present in vivo results are consistent with in vitro data showing less complex dendritic branching patterns in primary cultures of hippocampal neurons from CGG KI mice versus WT mice (Chen et al., 2010). Altered patterns of dendritic arborization and spine morphology may also reflect abnormal embryonic cortical development reported earlier by Cunningham et al. (2011) who documented abnormal migration and differentiation of embryonic neocortical precursor cells in CGG KI mice compared to WT mice.

A second mouse model of the PM has been described by Qin et al. (2011). This KI mouse also shows elevated *Fmr1* mRNA and reduced FMRP, although the reduction in FMRP in the Qin model is markedly greater than that observed in the KI mice used in the present study (i.e., 80–90% vs. 15–30% in the present CGG mouse model). The reasons for these differences between models are currently unknown, but clearly raise important new questions about the mechanisms underlying the reduction in FMRP associated with CGG repeat expansions on *Fmr1*. Consistent with the present findings, Qin et al. (2011) found reduced dendritic complexity in layer III pyramidal neurons in medial prefrontal cortex, CA3 region of the hippocampus, and basolateral amygdala, and increased dendritic spine length on both basal and apical dendrites in medial prefrontal cortex, hippocampus, and amygdala.

The molecular mechanisms underlying abnormal morphology of neurons in the CGG KI mice are unclear, but are likely to be associated with the elevated *Fmr1* mRNA and reduced FMRP in brain that characterize the fragile X premutation (Berman & Willemsen, 2009; Willemsen et al., 2011). Support for a role of FMRP in abnormal dendritic and spine morphology comes from human postmortem studies of the FXS and animal studies in the *Fmr1* KO mouse used to model FXS. Patients with FXS show complete or nearly complete absence of FMRP due to hyper-methylation of *Fmr1* resulting in silencing of transcription (Bell et al., 1991). These individuals develop mental retardation, and previous Golgi analyses of postmortem tissues from these individuals show abnormal dendritic spine density and spine morphology in temporal and visual neocortical pyramidal neurons (Hinton et al., 1991; Irwin et al., 2001). Fragile X patients showed an increase in dendritic spine density and an increase in the frequency of spines with immature “filipodial” morphology.

These morphologic features have been suggested to underlie impaired cognitive function associated with FXS (Irwin et al., 2002). Similarly, increased density and abnormal spine morphology have been found in the *Fmr1* KO mouse cortex (Irwin et al., 2002) and hippocampus (Grossman et al., 2010). Levenga et al. (2011) labeled dendritic spines of 25-week-old *Fmr1* KO mice with fluorescent DiI and also found more immature filipodia-like spines in hippocampal CA1, but not in CA3. Of interest, this abnormal spine morphology as well as abnormal sensory gating measured by prepulse inhibition (PPI) could be rescued by treatment with MPEP, an mGluR5 antagonist (de Vrij et al., 2008). The increase in spine density and immature spines suggests that both synaptic pruning and synapse maturation during development may be impaired in FXS. Additional support for a role for a reduction in FMRP in abnormal dendritic branching and spine morphology comes from studies showing that loss of FMRP is associated with defects in axonal growth cone dynamics and synaptic plasticity, as well as the fact FMRP appears to be located both presynaptically and postsynaptically (Antar et al., 2006; Bassell & Warren, 2008).

The present results show both similarities and differences from studies in *Fmr1* KO mice. Specifically, we find greater numbers of longer dendritic spines in layer II/III visual cortex in CGG KI mice compared to WT mice, and this is consistent with human (Hinton et al., 1991; Irwin et al., 2001) and rodent studies (Irwin et al., 2002; McKinney et al., 2005; Grossman et al., 2006, 2010). Our results differ from observations in *Fmr1* KO mice in that we did not find a specific increase in the proportion of immature filipodia-type spines (Irwin et al., 2001; McKinney et al., 2005; Grossman et al., 2010). In addition, we found significant reduction in the complexity of dendrite branching patterns, and this is not found in the *Fmr1* KO mouse (Irwin et al., 2002). To our knowledge dendritic branching patterns have not been examined in postmortem tissues from carriers of the PM or FXTAS patients, or in the FXS. We also found a decrease in total dendritic length in CGG KI compared to WT mice that appeared to be associated primarily with apical dendrites, and this morphologic difference has not been reported in FXS cases or *Fmr1* KO mice.

The argument that dendritic branching and spine anomalies may be due, wholly or in part, to a lack of FMRP is weakened by differences in the types of morphologic changes in dendrites and spines between CGG KI mice with only reduced levels of FMRP and the fragile X KO mouse completely lacking FMRP. Specifically, neocortical pyramidal neurons in both CGG KI mice and *Fmr1* KO mice show longer spines, suggesting that reduced FMRP in both mouse models could contribute to spine anomalies. However, increased spine density reported in FXS (Irwin et al., 2001) and in the *Fmr1* KO mouse (McKinney et al., 2005) was not seen in the present study in CGG KI mice. In addition, reduced complexity in the branching of dendritic arbors seen in CGG KI, and in hippocampal neurons in culture isolated from CGG KI mice (Chen et al., 2010), has not been found in *Fmr1* KO mice when examined (Irwin et al., 2002; de Vrij et al., 2008), and has not been reported in postmortem tissues from FXS. Therefore, it is possible that reduction in FMRP may underlie spine anomalies, whereas elevated *Fmr1* mRNA seen in the fragile X premutation, FXTAS, and CGG KI mice may contribute to abnormal dendritic branching patterns, but may not be as involved in abnormal development of dendritic spines. Indeed, elevated levels of *FMR1* mRNA have led to the proposal that the PM phenotype and FXTAS results from a toxic

"RNA gain of function" (Hagerman et al., 2001; Jin et al., 2003; Handa et al., 2005), where neuropathology is thought to be due to increased levels of expanded CGG mRNA sequestering specific RNA-binding proteins (e.g., Pur-α, hnRNPA2/ B1, CUGBP1, Sam68) that are important for normal cellular functions (e.g., mRNA transport, protein trafficking, alternative splicing, and microRNA processing) (Willemsen et al., 2011). Elegant studies have provided evidence of direct RNA toxicity by demonstrating at least partial rescue of the WT phenotype by overexpressing the sequestered protein candidates in the context of the expanded CGG-repeat RNA (Sellier, et al., 2011).

In conclusion, dendritic arborization and dendritic spine morphology appear to be abnormal in layer II/III of the primary visual cortex of the adult CGG KI mouse model of the PM and FXTAS. This includes a general decrease in the branching complexity of dendrites of pyramidal neurons, a decrease in total dendritic length, particularly for apical dendrites, and an increase in the proportion of longer dendritic spines. The longer dendritic spines were not specifically associated with immature- or mature-appearing spines. Dendritic spine density did not differ between WT and CGG KI mice. These results in CGG KI mice suggest that neuropathology in FXTAS reported in previous studies (e.g., loss of Purkinje cells, presence of intra nuclear protein inclusions, loss of myelination) may also include dendritic and spine abnormalities. Such studies have not been carried out in human postmortem tissues from FXTAS patients, but should be undertaken in the future. The relative roles of elevated *Fmr1* mRNA and decreased FMRP in pathology remain unclear, but differences in the morphologic changes seen between CGG KI mice with only slightly reduced levels of FMRP and CGG KO mice without any FMRP, suggest a role for elevated *Fmr1* mRNA in the observed dendrite and spine pathology. The present results are limited to primary visual cortex, and it is likely that other brain regions—including the hippocampus, amygdala, and cerebellum—will show abnormal dendritic and spine morphologies and that these studies also need to be undertaken to better understand the scope of pathology in the nervous system of CGG KI mice, and by analogy FXTAS. Finally, it is tempting to ascribe sensory, motor, and cognitive impairments in the PM and FXTAS to abnormal synaptic structure. However, this relationship has not yet been firmly established, and will probably require development of new mouse models of these disorders that will allow for direct experimenter control of *Fmr1* mRNA expression and levels of FMRP over the course of development of the nervous system, and such models are currently being developed.

Acknowledgments

This work was supported by National Institutes of Health (NIH) Grants, National Institute of Neurological Disorders and Stroke (NINDS) RL1 NS062411 and TL1 DA024854. This work was also made possible by a Roadmap Initiative Grant (UL1 DE019583) from the National Institute of Dental and Craniofacial Research (NIDCR) in support of the NeuroTherapeutics Research Institute (NTRI) consortium; and by a Grant (UL1 RR024146) from the National Center for Research Resources (NCRR), a component of the NIH, and NIH Roadmap for Medical Research.

The authors wish to thank Binh T. Ta for assistance with the genotyping of mice used in this study, Elizabeth Rognlie-Howes for managing the mouse colony, Emily T. Doisy and Carrie C. Poon for assistance with the neuronal reconstruction and dendritic spine analyses, and Ramona E. von Leden for assistance with western blotting.

Those of us who have been fortunate enough to work with Professor H. Jürgen Wenzel express our appreciation for his important contributions to the laboratory, to the research, and to the training of many postdoctoral, graduate, and

undergraduate students. Jürgen's remarkable knowledge and skill in neuroanatomy, and his unwavering insistence on excellence, have made their mark on our laboratory and raised the bar for quality for all of us. We also acknowledge his friendship, generosity, and camaraderie over the years. Very few individual can be said to be "world class" in their field—but Jürgen is clearly among that select few.

References

Antar LN, Li C, Zhang H, Carroll RC, Bassell GJ. Local functions for FMRP in axon growth cone motility and activity-dependent regulation of filopodia and spine synapses. Mol Cell Neurosci. 2006; 32:37–48. [PubMed: 16631377]

Bassell GJ, Warren ST. Fragile X syndrome: loss of local mRNA regulation alters synaptic development and function. Neuron. 2008; 60:201–214. [PubMed: 18957214]

Basuta K, Narcisa V, Chavez A, Kumar M, Gane L, Hagerman R, Tassone F. Clinical phenotypes of a juvenile sibling pair carrying the fragile X premutation. Am J Med Genet A. 2011; 155A:519–525. [PubMed: 21344625]

Bell MV, Hirst MC, Nakahori Y, MacKinnon RN, Roche A, Flint TJ, Jacobs PA, Tommerup N, Tranebjaerg L, Froster-Iskenius U, Kerr B, Turner G, Lindenbaum RH, Winter R, Pembrey M, Thibodeau S, Davies KE. Physical mapping across the fragile X: hypermethylation and clinical expression of the fragile X syndrome. Cell. 1991; 64:861–866. [PubMed: 1997211]

Berman RF, Willemsen R. Mouse models of fragile x-associated tremor ataxia. J Investig Med. 2009; 57:837–841.

Berry-Kravis E, Abrams L, Coffey SM, Hall DA, Greco C, Gane LW, Grigsby J, Bourgeois JA, Finucane B, Jacquemont S, Brunberg JA, Zhang L, Lin J, Tassone F, Hagerman PJ, Hagerman RJ, Leehey MA. Fragile X-associated tremor/ataxia syndrome: clinical features, genetics, and testing guidelines. Mov Disord. 2007a; 22:2018–2030. quiz 2140. [PubMed: 17618523]

Berry-Kravis E, Goetz CG, Leehey MA, Hagerman RJ, Zhang L, Li L, Nguyen D, Hall DA, Tartaglia N, Cogswell J, Tassone F, Hagerman PJ. Neuropathic features in fragile X premutation carriers. Am J Med Genet A. 2007b; 143:19–26. [PubMed: 17152065]

Bontekoe CJ, Bakker CE, Nieuwenhuizen IM, van der Linde H, Lans H, de Lange D, Hirst MC, Oostra BA. Instability of a (CGG)98 repeat in the *Fmr1* promoter. Hum Mol Genet. 2001; 10:1693–1699. [PubMed: 11487573]

Bourgeois JA, Cogswell JB, Hessl D, Zhang L, Ono MY, Tassone F, Farzin F, Brunberg JA, Grigsby J, Hagerman RJ. Cognitive, anxiety and mood disorders in the fragile X-associated tremor/ataxia syndrome. Gen Hosp Psychiatry. 2007; 29:349–356. [PubMed: 17591512]

Bourgeois JA, Coffey SM, Rivera SM, Hessl D, Gane LW, Tassone F, Greco C, Finucane B, Nelson L, Berry-Kravis E, Grigsby J, Hagerman PJ, Hagerman RJ. A review of fragile X premutation disorders: expanding the psychiatric perspective. J Clin Psychiatry. 2009; 70:852–862. [PubMed: 19422761]

Braun K, Segal M. FMRP involvement in formation of synapses among cultured hippocampal neurons. Cereb Cortex. 2000; 10:1045–1052. [PubMed: 11007555]

Brouwer JR, Huizer K, Severijnen LA, Hukema RK, Berman RF, Oostra BA, Willemsen R. CGG-repeat length and neuropathological and molecular correlates in a mouse model for fragile X-associated tremor/ataxia syndrome. J Neurochem. 2008; 107:1671–1682. [PubMed: 19014369]

Brunberg JA, Jacquemont S, Hagerman RJ, Berry-Kravis EM, Grigsby J, Leehey MA, Tassone F, Brown WT, Greco CM, Hagerman PJ. Fragile X premutation carriers: characteristic MR imaging findings of adult male patients with progressive cerebellar and cognitive dysfunction. AJNR Am J Neuroradiol. 2002; 23:1757–1766. [PubMed: 12427636]

Chen Y, Tassone F, Berman RF, Hagerman PM, Hagerman RJ, Willemsen R, Pessah IN. Murine hippocampal neurons expressing *Fmr1* gene premutation show early developmental deficits and late degeneration. Hum Mol Genet. 2010; 19:196–208. [PubMed: 19846466]

Chonchaiya W, Au J, Schneider A, Hessl D, Harris SW, Laird M, Mu Y, Tassone F, Nguyen DV, Hagerman RJ. Increased prevalence of seizures in boys who were probands with the *FMR1* premutation and co-morbid autism spectrum disorder. Hum Genet. 2012; 131:581–589. [PubMed: 22001913]

Cunningham CL, Martinez Cerdeno V, Navarro Porras E, Prakash AN, Angelastro JM, Willemsen R, Hagerman PJ, Pessah IN, Berman RF, Noctor SC. Premutation CGG-repeat expansion of the *Fmr1* gene impairs mouse neocortical development. Hum Mol Genet. 2011; 20:64–79. [PubMed: 20935171]

de Vrij FM, Levenga J, van der Linde HC, Koekkoek SK, De Zeeuw CI, Nelson DL, Oostra BA, Willemsen R. Rescue of behavioral phenotype and neuronal protrusion morphology in *Fmr1* KO mice. Neurobiol Dis. 2008; 31:127–132. [PubMed: 18571098]

Goodrich-Hunsaker NJ, Wong LM, McLennan Y, Srivastava S, Tassone F, Harvey D, Rivera SM, Simon TJ. Young adult female fragile X premutation carriers show age- and genetically-modulated cognitive impairments. Brain Cogn. 2011a; 75:255–260. [PubMed: 21295394]

Goodrich-Hunsaker NJ, Wong LM, McLennan Y, Tassone F, Harvey D, Rivera SM, Simon TJ. Adult female fragile X premutation carriers exhibit age- and CGG repeat length-related impairments on an attentionally based enumeration task. Front Hum Neurosci. 2011b; 5:63. [PubMed: 21808616]

Goodrich-Hunsaker NJ, Wong LM, McLennan Y, Tassone F, Harvey D, Rivera SM, Simon TJ. Enhanced manual and oral motor reaction time in young adult female fragile X premutation carriers. J Int Neuropsychol Soc. 2011c; 21:1–5.

Greco CM, Berman RF, Martin RM, Tassone F, Schwartz PH, Chang A, Trapp BD, Iwahashi C, Brunberg J, Grigsby J, Hessl D, Becker EJ, Papazian J, Leehey MA, Hagerman RJ, Hagerman PJ. Neuropathology of fragile X-associated tremor/ataxia syndrome (FXTAS). Brain. 2006; 129:243–255. [PubMed: 16332642]

Grossman AW, Elisseou NM, McKinney BC, Greenough WT. Hippocampal pyramidal cells in adult Fmr1 knockout mice exhibit an immature-appearing profile of dendritic spines. Brain Res. 2006; 1084:158–164. [PubMed: 16574084]

Grossman AW, Aldridge GM, Lee KJ, Zeman MK, Jun CS, Azam HS, Arii T, Imoto K, Greenough WT, Rhyu IJ. Developmental characteristics of dendritic spines in the dentate gyrus of Fmr1 knockout mice. Brain Res. 2010; 1355:221–227. [PubMed: 20682298]

Hagerman PJ. The fragile X prevalence paradox. J Med Genet. 2008; 45:498–499. [PubMed: 18413371]

Hagerman RJ, Hagerman PJ. Testing for fragile X gene mutations throughout the life span. JAMA. 2008; 300:2419–2421. [PubMed: 19033593]

Hagerman RJ, Leehey M, Heinrichs W, Tassone F, Wilson R, Hills J, Grigsby J, Gage B, Hagerman PJ. Intention tremor, parkinsonism, and generalized brain atrophy in male carriers of fragile X. Neurology. 2001; 57:127–130. [PubMed: 11445641]

Hagerman RJ, Leavitt BR, Farzin F, Jacquemont S, Greco CM, Brunberg JA, Tassone F, Hessl D, Harris SW, Zhang L, Jardini T, Gane LW, Ferranti J, Ruiz L, Leehey MA, Grigsby J, Hagerman PJ. Fragile-X-associated tremor/ataxia syndrome (FXTAS) in females with the FMR1 premutation. Am J Hum Genet. 2004; 74:1051–1056. [PubMed: 15065016]

Handa V, Goldwater D, Stiles D, Cam M, Poy G, Kumari D, Usdin K. Long CGG-repeat tracts are toxic to human cells: implications for carriers of Fragile X premutation alleles. FEBS Lett. 2005; 579:2702–2708. [PubMed: 15862312]

Hantash FM, Goos DM, Crossley B, Anderson B, Zhang K, Sun W, Strom CM. FMR1 premutation carrier frequency in patients undergoing routine population-based carrier screening: insights into the prevalence of fragile X syndrome, fragile X-associated tremor/ataxia syndrome, and fragile X-associated primary ovarian insufficiency in the United States. Genet Med. 2011; 13:39–45. [PubMed: 21116185]

Hessl D, Tassone F, Loesch DZ, Berry-Kravis E, Leehey MA, Gane LW, Barbato I, Rice C, Gould E, Hall DA, Grigsby J, Wegelin JA, Harris S, Lewin F, Weinberg D, Hagerman PJ, Hagerman RJ. Abnormal elevation of FMR1 mRNA is associated with psychological symptoms in individuals with the fragile X premutation. Am J Med Genet B Neuropsychiatr Genet. 2005; 139:115–121. [PubMed: 16184602]

Hinton VJ, Brown WT, Wisniewski K, Rudelli RD. Analysis of neocortex in three males with the fragile X syndrome. Am J Med Genet. 1991; 41:289–294. [PubMed: 1724112]

Huber KM, Gallagher SM, Warren ST, Bear MF. Altered synaptic plasticity in a mouse model of fragile X mental retardation. Proc Natl Acad Sci U S A. 2002; 99:7746–7750. [PubMed: 12032354]

Hunsaker MR, Wenzel HJ, Willemsen R, Berman RF. Progressive spatial processing deficits in a mouse model of the fragile X premutation. Behav Neurosci. 2009; 123:1315–1324. [PubMed: 20001115]

Hunsaker MR, Goodrich-Hunsaker NJ, Willemsen R, Berman RF. Temporal ordering deficits in female CGG KI mice heterozygous for the fragile X premutation. Behav Brain Res. 2010; 213:263–268. [PubMed: 20478339]

Hunsaker MR, von Leden RE, Ta BT, Goodrich-Hunsaker NJ, Arque G, Kim K, Willemsen R, Berman RF. Motor deficits on a ladder rung task in male and female adolescent and adult CGG knock-in mice. Behav Brain Res. 2011; 222:117–121. [PubMed: 21440572]

Irwin SA, Patel B, Idupulapati M, Harris JB, Crisostomo RA, Larsen BP, Kooy F, Willems PJ, Cras P, Kozlowski PB, Swain RA, Weiler IJ, Greenough WT. Abnormal dendritic spine characteristics in the temporal and visual cortices of patients with fragile-X syndrome: a quantitative examination. Am J Med Genet. 2001; 98:161–167. [PubMed: 11223852]

Irwin SA, Idupulapati M, Gilbert ME, Harris JB, Chakravarti AB, Rogers EJ, Crisostomo RA, Larsen BP, Mehta A, Alcantara CJ, Patel B, Swain RA, Weiler IJ, Oostra BA, Greenough WT. Dendritic spine and dendritic field characteristics of layer V pyramidal neurons in the visual cortex of fragile-X knockout mice. Am J Med Genet. 2002; 111:140–146. [PubMed: 12210340]

Iwahashi CK, Yasui DH, An HJ, Greco CM, Tassone F, Nannen K, Babineau B, Lebrilla CB, Hagerman RJ, Hagerman PJ. Protein composition of the intranuclear inclusions of FXTAS. Brain. 2006; 129:256–271. [PubMed: 16246864]

Iwahashi C, Tassone F, Hagerman RJ, Yasui D, Parrott G, Nguyen D, Mayeur G, Hagerman PJ. A quantitative ELISA assay for the fragile x mental retardation 1 protein. J Mol Diagn. 2009; 11:281–289. [PubMed: 19460937]

Jacquemont S, Hagerman RJ, Leehey MA, Hall DA, Levine RA, Brunberg JA, Zhang L, Jardini T, Gane LW, Harris SW, Herman K, Grigsby J, Greco CM, Berry-Kravis E, Tassone F, Hagerman PJ. Penetrance of the fragile X-associated tremor/ataxia syndrome in a premutation carrier population. JAMA. 2004; 291:460–469. [PubMed: 14747503]

Jin P, Zarnescu DC, Zhang F, Pearson CE, Lucchesi JC, Moses K, Warren ST. RNA-mediated neurodegeneration caused by the fragile X premutation rCGG repeats in Drosophila. Neuron. 2003; 39:739–747. [PubMed: 12948442]

Keri S, Benedek G. The perception of biological and mechanical motion in female fragile X premutation carriers. Brain Cogn. 2010; 72:197–201. [PubMed: 19766375]

Kogan CS, Cornish KM. Mapping self-reports of working memory deficits to executive dysfunction in Fragile X Mental Retardation 1 (FMR1) gene premutation carriers asymptomatic for FXTAS. Brain Cogn. 2010; 73:236–243. [PubMed: 20573435]

Lachiewicz A, Dawson D, Spiridigliozzi G, Cuccaro M, Lachiewicz M, McConkie-Rosell A. Indicators of anxiety and depression in women with the fragile X premutation: assessment of a clinical sample. J Intellect Disabil Res. 2010; 54:597–610. [PubMed: 20629912]

Leehey MA, Berry-Kravis E, Goetz CG, Zhang L, Hall DA, Li L, Rice CD, Lara R, Cogswell J, Reynolds A, Gane L, Jacquemont S, Tassone F, Grigsby J, Hagerman RJ, Hagerman PJ. FMR1 CGG repeat length predicts motor dysfunction in premutation carriers. Neurology. 2008; 70:1397–1402. [PubMed: 18057320]

Levenga J, de Vrij FM, Buijsen RA, Li T, Nieuwenhuizen IM, Pop A, Oostra BA, Willemsen R. Subregion-specific dendritic spine abnormalities in the hippocampus of Fmr1 KO mice. Neurobiol Learn Mem. 2011; 95:467–472. [PubMed: 21371563]

McKinney BC, Grossman AW, Elisseou NM, Greenough WT. Dendritic spine abnormalities in the occipital cortex of C57BL/6 Fmr1 knockout mice. Am J Med Genet B Neuropsychiatr Genet. 2005; 136B:98–102. [PubMed: 15892134]

Qin M, Entezam A, Usdin K, Huang T, Liu ZH, Hoffman GE, Smith CB. A mouse model of the fragile X premutation: effects on behavior, dendrite morphology, and regional rates of cerebral protein synthesis. Neurobiol Dis. 2011; 42:85–98. [PubMed: 21220020]

Raske C, Hagerman PJ. Molecular pathogenesis of fragile X-associated tremor/ataxia syndrome. J Investig Med. 2009; 57:825–829.

Sellier C, Rau F, Liu Y, Tassone F, Hukema RK, Gattoni R, Schneider A, Richard S, Willemsen R, Elliott DJ, Hagerman PJ, Charlet-Berguerand N. Sam68 sequestration and partial loss of function are associated with splicing alterations in FXTAS patients. EMBO J. 2010; 29:1248–1261. [PubMed: 20186122]

Sholl DA. Dendritic organization in the neurons of the visual and motor cortices of the cat. J Anat. 1953; 87:387–406. [PubMed: 13117757]

Stratford KJ, Jack JJ, Larkman AU. Calibration of an autocorrelation-based method for determining amplitude histogram reliability and quantal size. J Physiol. 1997; 505(Pt 2):425–442. [PubMed: 9423184]

Tassone F, Hagerman RJ, Garcia-Arocena D, Khandjian EW, Greco CM, Hagerman PJ. Intranuclear inclusions in neural cells with premutation alleles in fragile X associated tremor/ataxia syndrome. J Med Genet. 2004; 41:e43. [PubMed: 15060119]

Tassone F, Beilina A, Carosi C, Albertosi S, Bagni C, Li L, Glover K, Bentley D, Hagerman PJ. Elevated FMR1 mRNA in premutation carriers is due to increased transcription. RNA. 2007; 13:555–562. [PubMed: 17283214]

Van Dam D, Errijgers V, Kooy RF, Willemsen R, Mientjes E, Oostra BA, De Deyn PP. Cognitive decline, neuromotor and behavioural disturbances in a mouse model for fragile-X-associated tremor/ataxia syndrome (FXTAS). Behav Brain Res. 2005; 162:233–239. [PubMed: 15876460]

Wenzel HJ, Hunsaker MR, Greco CM, Willemsen R, Berman RF. Ubiquitin-positive intranuclear inclusions in neuronal and glial cells in a mouse model of the fragile X premutation. Brain Res. 2010; 1318:155–166. [PubMed: 20051238]

Willemsen R, Hoogeveen-Westerveld M, Reis S, Holstege J, Severijnen LA, Nieuwenhuizen IM, Schrier M, van Unen L, Tassone F, Hoogeveen AT, Hagerman PJ, Mientjes EJ, Oostra BA. The FMR1 CGG repeat mouse displays ubiquitin-positive intranuclear neuronal inclusions; implications for the cerebellar tremor/ataxia syndrome. Hum Mol Genet. 2003; 12:949–959. [PubMed: 12700164]

Willemsen R, Levenga J, Oostra BA. CGG repeat in the FMR1 gene: size matters. Clin Genet. 2011; 80:214–225. [PubMed: 21651511]

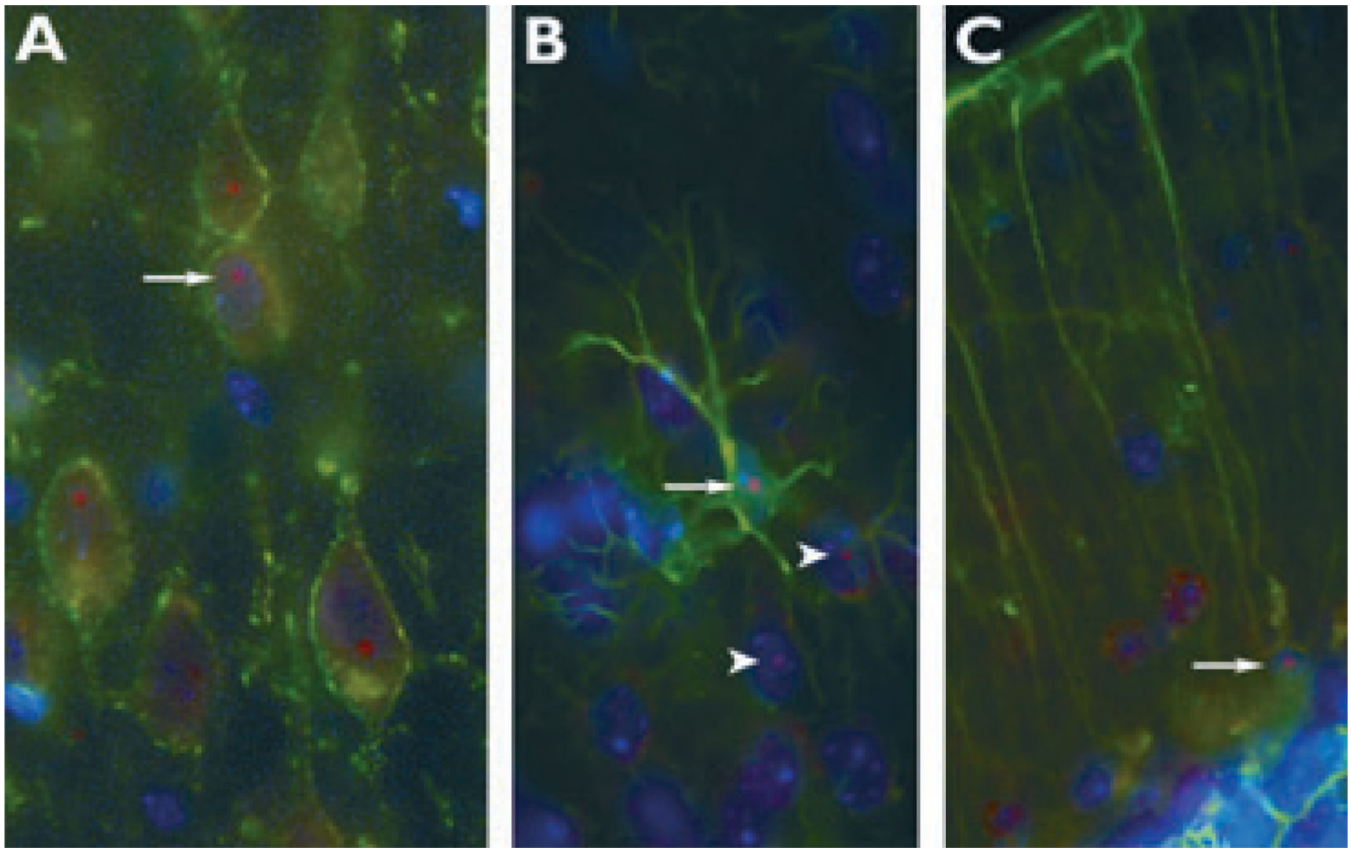

Figure 1.

Immunofluorescent photomicrographs of ubiquitinpositive intranuclear inclusions (arrows) immunolabeled in red. (**A**) Pyramidal neurons in motor cortex (green immunolabel for Kv2.1 potassium channels), (**B**) lamina I neocortical astrocytes (green immunolabel for GFAP), and (**C**) Bergmann glia (green immunolabel for GFAP) of CGG KI mice. In (**B**), note several intra-nuclear inclusions in adjacent neurons (arrowheads). Nuclei were stained with DAPI. (Adapted from Wenzel et al., 2010).

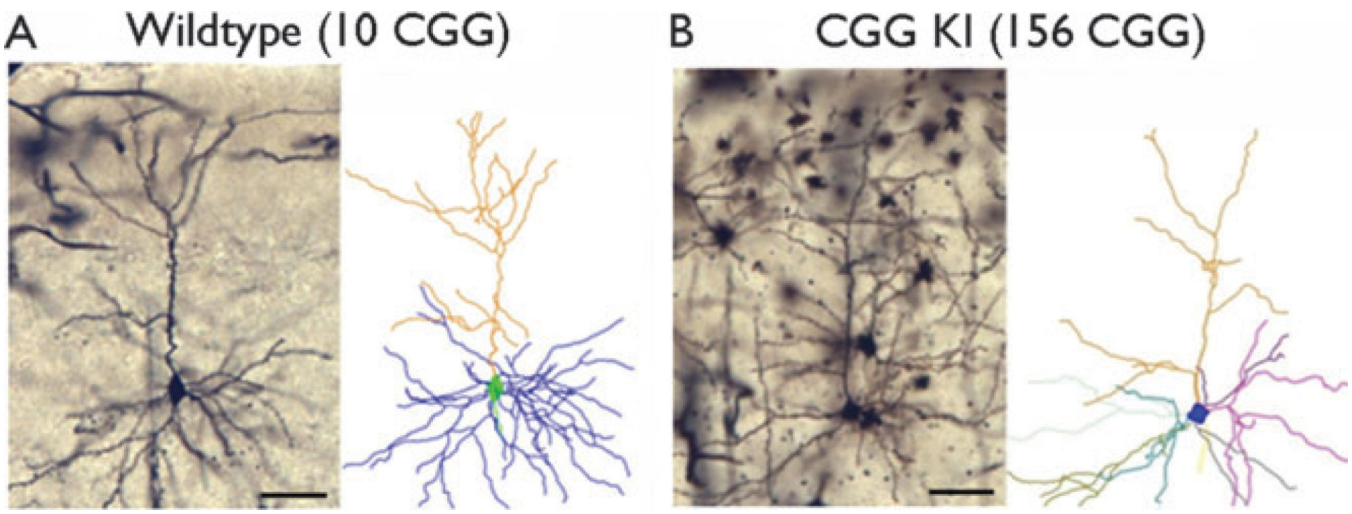

Figure 2.

Dendrite branching complexity. Representative reconstructions of dendritic arborization in layers II/III of primary visual cortex from WT (**A**) and CGG KI (**B**) mice with 10 (normal) or 156 CGG repeats (expanded) on *Fmr1*, respectively. Subsequent quantitative measures were made on similar reconstructions using Neurolucida software, including Sholl analysis for dendritic complexity (Sholl, 1953). Bar = 50 μm.

Epilepsia © ILAE

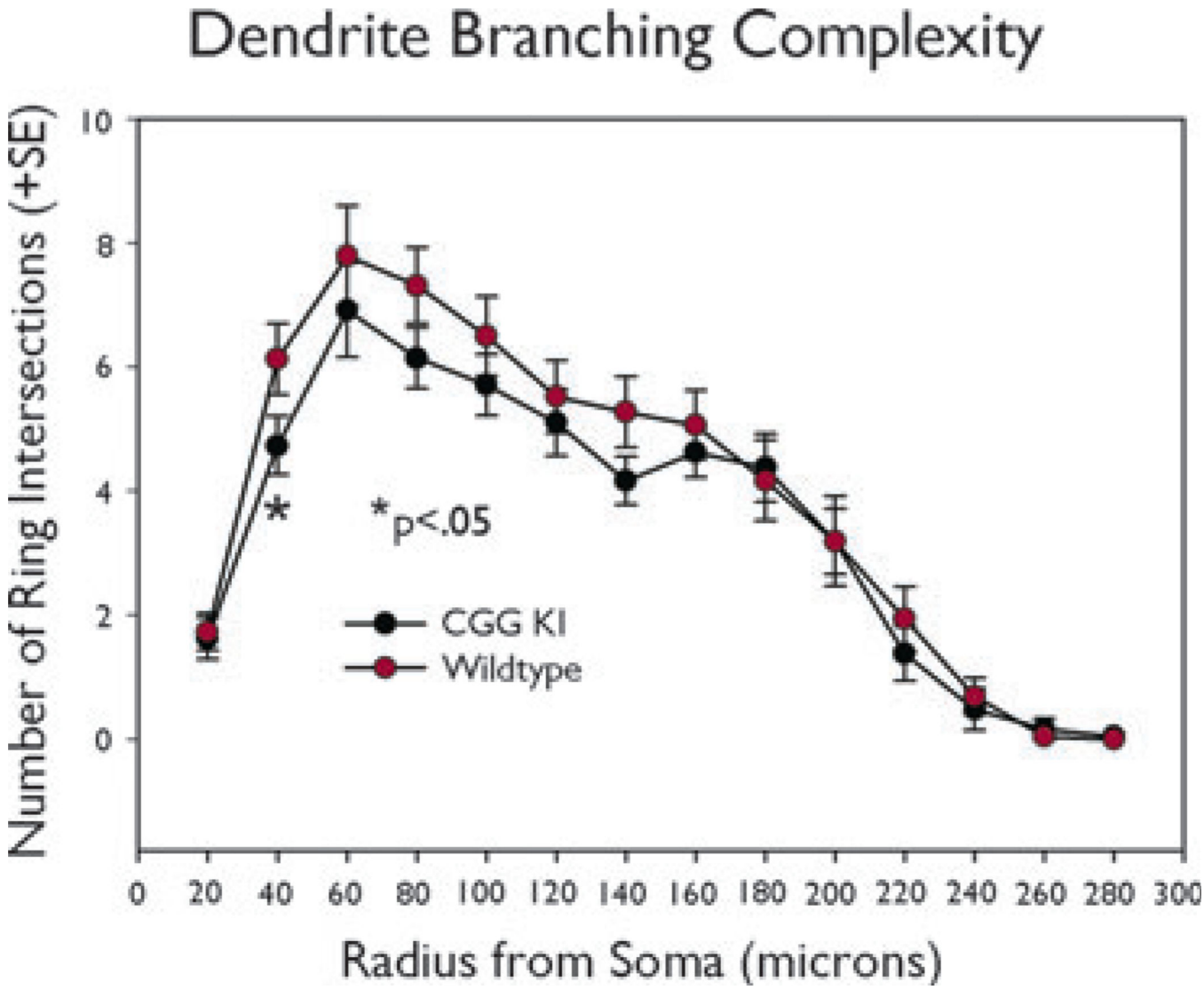

Figure 3.

Branching complexity of apical and basilar dendrites were quantified by Sholl analysis as the number of ring intersections by dendritic branches with ring diameter set at 20 μm (i.e., ring intersections/20 μm). The overall pattern of branching was less complex for CGG KI mice, and dendrites at 40 μm showed significantly fewer branches in CGG KI mice compared to WT mice ($p < 0.05$).

Epilepsia © ILAE

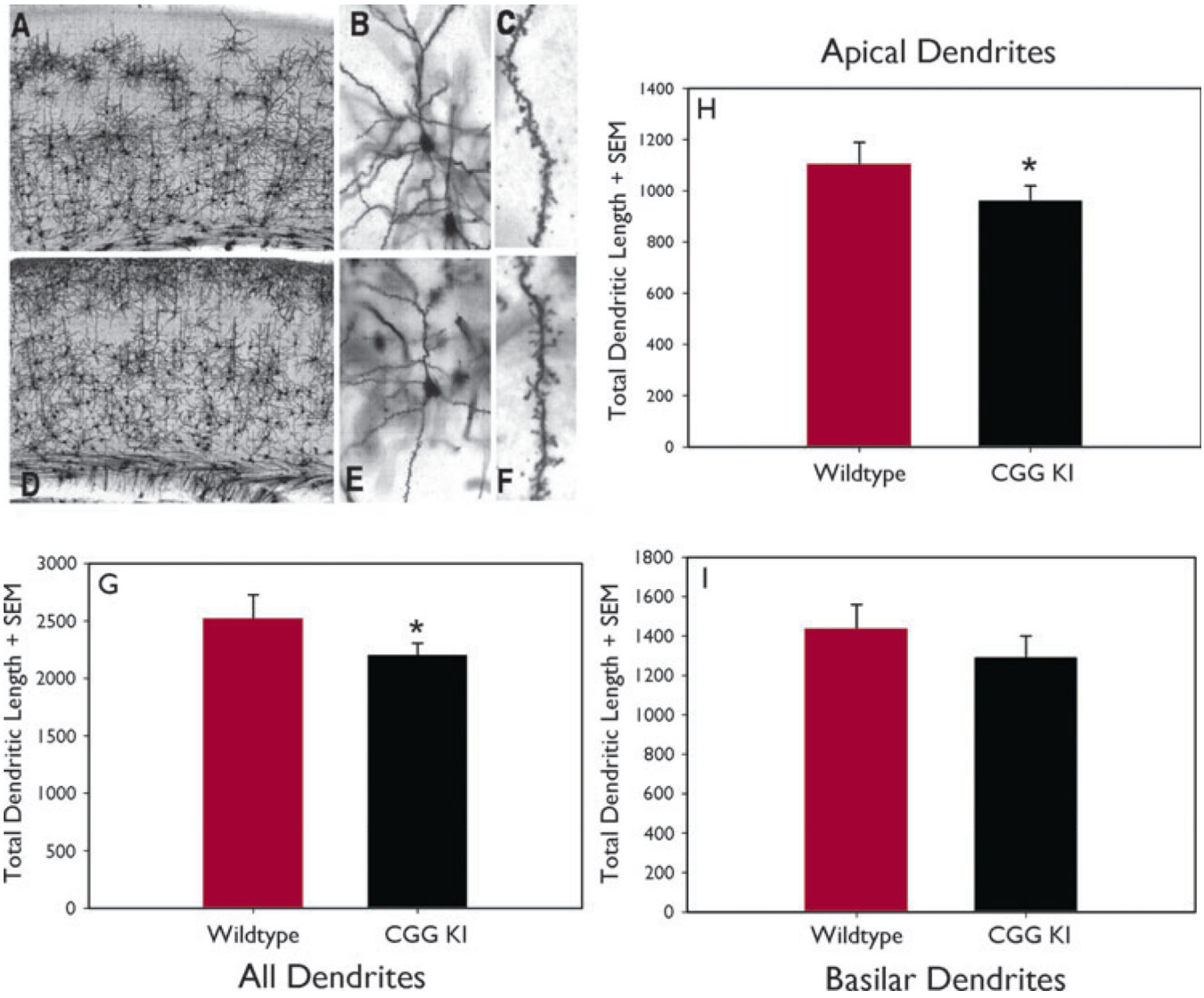

Figure 4.

Representative photomicrographs of Golgi-Cox stained pyramidal neurons in layer II/III of primary visual cortex of WT (**A, B, C**) and CGG KI mice (**D, E, F**) at progressively higher magnification. Total dendritic length was calculated from reconstructed dendritic arbors using Neurolucida software. Total dendritic length (**G**) was reduced for all dendrites ($p < 0.05$), but was only significantly reduced for apical dendrites ($p < 0.05$) when apical (**H**) and basilar (**I**) dendrites were analyzed separately. Magnification: **A** & **D** – 4×, **B** & **E** – 20×, **C** & **F** – 100×.

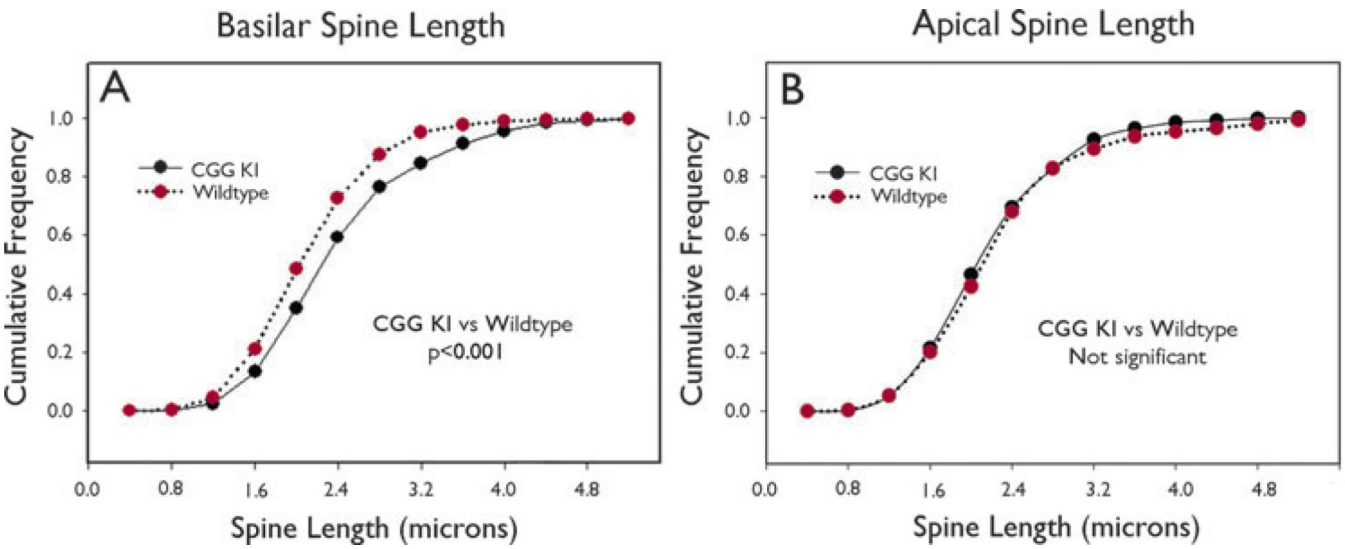

Figure 5.

Dendritic spine length for basilar (**A**) and apical (**B**) dendrites graphed as cumulative frequency distributions across spine lengths (0.4–5.2 μm). Overall mean spine lengths were significantly longer for CGG KI mice versus WT mice for basilar, but not apical dendrites ($p < 0.001$; Kolmogorov-Smirnov test).

Epilepsia © ILAE

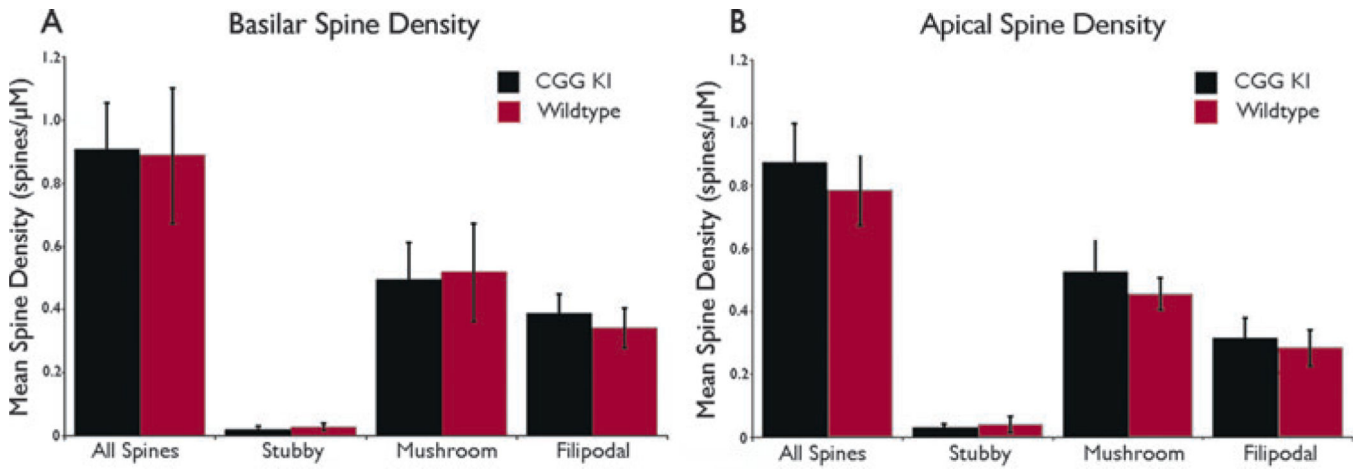

Figure 6.

Dendritic spines were classified according to shape (i.e., stubby, mushroom, filipodial) and spine density for each shape was determined for basilar (**A**) and apical (**B**) dendrites. There were no significant differences between CGG KI and WT mice in spine density.

Epilepsia © ILAE

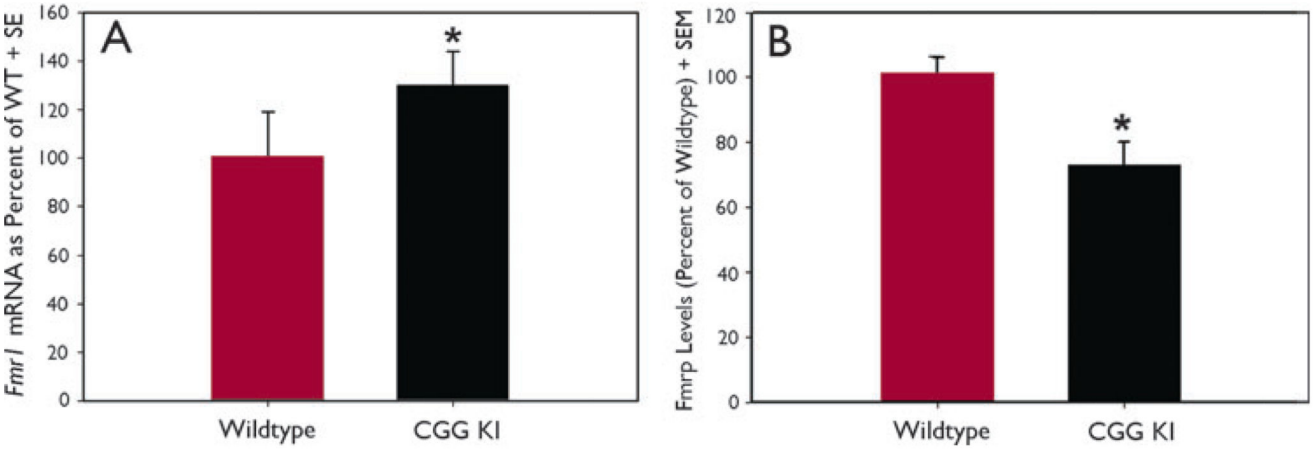

Figure 7.

(**A**) *Fmr1* mRNA expression levels were significant elevated by approximately 1.5-fold in adult male CGG KI mice compared to WT mice (*$p < 0.05$). (**B**) Whole brain levels of FMRP were decreased in CGG KI mice by approximately 28% compared to WT mice (*$p < 0.05$).

Epilepsia © ILAE

Table 1

Comparison of FXTAS with CGG KI mouse model[a]

Core pathology	Human FXTAS	CGG KI mouse
CGG trinucleotide repeat expansion length on *FMR1*	55–200 CGG repeat length, repeat instability	70–300 CGG repeat length, modest repeat instability
Elevated *FMR1* mRNA expression	2–8-fold increase	1.5–3.0-fold increase
FMRP levels	Reduced in several brain regions	Reduced in several brain regions
Motor impairment	Tremor/ataxia, postural sway, parkinsonism	Impaired on Rotorod, ladder rung task
Cognitive impairment	Poor working memory, anxiety, depression, social phobia	Spatial memory deficits, anxiety in elevated plus maze
Intranuclear inclusions	Neurons and astrocytes, highly correlated with CGG repeat length, frequency increases with aging	Neurons and astrocytes, related to length of CGG repeat, frequency increases with aging

[a] Adapted from Berman & Willemsen, 2009.